First-principles study on metal-doped icosahedral B_{12} solids

Shigeki Gunji* and Hiroshi Kamimura
Department of Applied Physics, Science University of Tokyo, 1-3 Kagurazaka, Shinjuku-ku, Tokyo 162, Japan
(Received 1 August 1995; revised manuscript received 29 March 1996)

Theoretical exploration of a group of ''C_{60}-like'' B_{12}-based materials, A_xB_{12}, with $A=$(Li and Ca) and $x=1-4$, is made by performing local-density approximation Gaussian basis calculations of the total energy, heats of formation, lattice constant, electronic structure, density of states, and bulk modulus of the putative compounds, using *ab initio* pseudopotentials. Lithium-doped materials are mostly demonstrated to give sufficient heats of formation, whereas it is shown that all Ca-doped materials are unstable, including Li_2CaB_{12}. Results are presented only for the stable and metastable Li_xB_{12} and compared with other current theoretical calculations on K_3C_{60}. The possibility of superconductivity is also discussed. The band-structure calculations reveal essentially metallic behavior of Li_xB_{12}. Important differences are found in the energy band structures, particularly in bands near the Fermi level, that would be reflected in superconductivity of these systems. Favorable superconducting properties are expected for Li_3B_{12}, in the context of sufficiently high $N(E_F)$ and obtained bulk modulus that is indicative of strong electron-phonon coupling. [S0163-1829(96)04440-2]

I. INTRODUCTION

All pristine boron (B) crystals have molecularly based structures. Some of them have a drastic similarity to the fcc solid C_{60}. The achievement of moderately high transition temperatures in the A_xC_{60} superconductors suggests that a superconducting phase may appear by metal doping into such semiconducting B solids. Especially for T_c, a high value is also expected, originated from the interaction of conduction electrons with high-frequency phonons caused by B-B covalent bondings. The recent discovery of superconductivity at 23 K in a Y-Pd-B-C quaternary alloy[1] also illustrates the importance of exploring boron compounds as a candidate for a superconductor. In this paper, a theoretical prediction is made on stability of new boron intercalation compounds together with their electronic structures and an investigation on superconductivity is also presented based on them.

The α-rhombohedral boron (α-rh B) has a structure of slightly compressed fcc rhombohedral primitive cell along the body-diagonal (111) direction (the c axis in the hexagonal description) and an icosahedral cluster occupies each vertex [cf. Fig. 1(a)]. This crystal is comparable to the fcc phase of solid C_{60}, as to both the translational and rotational symmetry. Iwasa *et al.* have recently reported a two-dimensional (2D) C_{60} polymer,[2] which is suggested to have a rhombohedral structure.[3] Its covalent-bonding-type cohesion and rhombohedral ordering of molecules indicate much closer resemblance between α-rh B and C_{60}-based solids. Only the 2D intermolecular bonding profile is different from 3D fcc-like network[4] of icosahedral clusters in α-rh B.

Icosahedral cluster in α-rh B is an almost regular icosahedron B_{12} where twelve B atoms arrange at all the vertices of the icosahedron [cf. Fig. 1(b)]. This icosahedron is distorted in its crystal forms,[5,6] reducing its symmetry from I_h to D_{3d}. The remaining D_{3d} symmetry divides twelve B atoms into four groups, i.e., two polar triangles [t and t^* in Fig. 1(b)] and two equatorial triangles [e and e^* in Fig. 1(b)]. The intramolecular cohesion mechanism is a three-center covalent bonding type, where the highest amplitude of the total charge density distribution appears near the center of a triangular face of the icosahedron. Each B atom has an additional radial p_π bond pointing outward from B_{12} in the direction of every fivefold axis. These p_π orbitals are bonded together between the nearest-neighbor B_{12} and form two types of covalent crystals, α-rh and β-rh B.

The β-rh B also has a rhombohedral unit cell, but rather

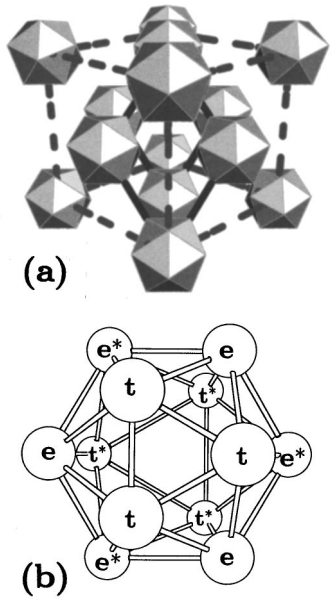

FIG. 1. Schematic views of (a) nearly fcc α-rh B crystal and (b) its icosahedral component, B_{12} cluster. The solid lines in (a) designate a rhombohedral primitive unit cell. The boron icosahedron is distorted, reducing its symmetry from I_h to D_{3d}. The remaining D_{3d} symmetry divides twelve B atoms into four groups, i.e., two polar triangles [t and t^* in (b)] and two equatorial triangles [e and e^* in (b)]. This threefold axis corresponds to the (111) direction. Note that intra-B_{12} bondings in (b) are drawn for convenience and are different from the actual multicenter bondings.

TABLE I. Estimated site radius by means of a simple rigid sphere model calculation. We also give the ionic radius of alkali and alkaline-earth-metal ions. Li^+, Na^+, and Ca^{2+} ions are small enough to occupy all of the sites.

Site	Radius (Å)	Element	Ionic radius (Å)	Element	Ionic radius (Å)
O	1.245	Li^+	0.60		
T_d	1.167	Na^+	0.95 [a]		
int	1.032	K^+	1.33 [a]	Ca^{2+}	0.99 [a]
B_{12} center	0.826	Rb^+	1.48 [a]	Sr^{2+}	1.13 [a]

[a]Reference 19.

elongated along the (111) direction. In this crystalline phase, the corners and the medium points of the edges are all occupied by B_{12} icosahedra. In addition to these clusters, a single B atom locates at the center of the unit cell that corresponds to the octahedral site in fcc crystal and two aggregates of three icosahedra are arranged symmetrically to it, along the major body-diagonal.[6] The β-rh B is a high-temperature phase above the α-rh phase and can easily be prepared in experiments compared with α-rh B because the melting point in B solids is as high as 2365 K,[7] whereas α-rh B is stable below 1370 K.[8] A metal doping to β-rh B is also of interest, but the crystalline complexity and already occupied octahedral sites are expected to give rise to a different situation, as compared to the doped C_{60}. We have thus chosen the α-rh B as a parent material in spite of the experimental difficulty. An *ab initio* prediction of a new material requires considerable CPU time, but it allows greater opportunity to clarify the physical quantities of materials, especially of these kinds of compounds that are hard to be synthesized by experiments. Working with another fcc system composed of icosahedra also leads to a better understanding of structural influence over the physical properties in A_xC_{60}.

In our previous papers,[9–12] we have pointed out the possible existence of α-rh B derivatives Li_xB_{12} ($x=1$–3). We simply calculated their electronic structures with use of density-functional formalism within local-density approximation (LDA), without considering any geometrical optimizations of α-rh B. However, most of electronic properties near the Fermi level are particularly sensitive to the structural relaxation and need to be more precisely evaluated especially for a discussion on superconductivity. For example, the density of states at Fermi level has increased by 15–19 % in optimized structure, compared with unrelaxed structure. We will explain it later in Sec. IV C.

One of the aims of this paper is to give accurate electronic structure studies on these materials at their optimized structure and also to present an analysis of superconductivity based on them. A preliminary report has been given only for Li_3B_{12}.[12] The other aim of this paper is to study more extensive A_xB_{12} systems ($A=$Li or Ca; $x=1$–4). In this paper, we investigate $Li@Li_3B_{12}$, $Li@B_{12}$, Ca_xB_{12}, and $Li_{1-x}Ca_xB_{12}$. We first clarify their stability and then present their electronic structure and possibility of superconductivity, only for the stable materials, at their optimized geometry.

II. MODELS

The α-rh B is of interest as a parent material of new compounds since it has a number of interstices inside. The already known boron-rich solids, boron carbide ($B_{12}C_3$),[13,14] boron phosphide ($B_{12}P_2$),[13–15] and boron arsenide ($B_{12}As_2$),[13–15] are regarded as α-rh B derivatives, where C, P, or As atoms are respectively inserted into these interstices of α-rh B. They show a striking feature in observed band-gap energies,[15–17] which widely change from infrared to ultraviolet region. However, no experimental studies on metal-doped α-rh B have been reported so far. It has raised two fundamental questions in investigating metal doped α-rh B theoretically. The first one is at which position the metals should be doped and the second one is how the α-rh B unit cell is deformed in size and/or shape by dopings. To respond to these questions, we assume the following four realistic sites. Then the stability is analyzed with allowing lattice relaxations: (a) an octahedral (O) site that corresponds to the body center in the unit cell of α-rh B, (b) two tetrahedral (T_d) sites per unit cell, (c) both ends of an interstitial chain along the longest body diagonal that equal P positions in $B_{12}P_2$ [called interstitial (int) sites], and (d) the center of the hollow cluster B_{12}, which we have not dealt with in the previous papers.

Geometrical conditions of α-rh B are like those of pristine fcc C_{60}, but the intermolecular cohesion mechanism is quite different. In contrast to the intermolecular van der Waals cohesion in fullerite, intermolecular coupling in α-rh B is of a covalent bonding type due to transfer interactions between neighboring B_{12} icosahedra. It is therefore hard to dope relatively heavy alkali or alkaline-earth metals of large ionic radius into α-rh B. In order to aid a construction of our models, we have calculated the site radius based on a simple rigid-sphere model, using available experimental information[13,14,18] on α-rh B and $B_{12}P_2$. The structural data of α-rh B and $B_{12}P_2$ are given in Ref. 10. The atomic radius of the B atom required in our calculation has been estimated from the experimental B-B covalent bond length, which is approximately 0.88 Å on the average. The calculated results are summarized in Table I, together with the ionic radius of alkali- and alkaline-earth-metal ions given by Pauling.[19] In our analysis, the IIA elements Be^{2+} and Mg^{2+} are not investigated in spite of the small values in ionic radius because their chemical property is quite different from others.

The spheres of the four sites range over 0.826−1.245 Å in radius, according as the order of $O>T_d>int>B_{12}$ center. We have also found out that even the most spacious O site can only accommodate relatively small ions, such as Li^+, Na^+, Ca^{2+}, and Sr^{2+}. Thus the smallest alkali metal Li and the smallest alkaline-earth metal Ca have been chosen as dopants.

Depending on the positions and concentration, the realistic model systems $LiB_{12}(O)$, $Li_2B_{12}(T_d)$, $Li_2B_{12}(int)$, and $Li@B_{12}$ are constructed for Li-doping case. On each of the systems, a numerical work has proceeded in a way that we will describe in Sec. III. The structural formula $LiB_{12}(O)$ represents the case that Li atoms are doped into every O site. In $Li_2B_{12}(T_d)$ or $Li_2B_{12}(int)$, Li atoms (two per unit cell) are doped into T_d or interstitial sites, respectively. The formula $Li@B_{12}$ represents the case that Li atoms occupy the centers of all the B_{12} clusters. Based on the total-energy analysis, we have also investigated other systems in the same way, which corresponds to Li doping into more than one kind of the above-mentioned four sites at a time, including Li_3B_{12}, the same way of doping as the superconducting composition A_3C_{60}. The Ca-doping cases, including $Li_{3-x}Ca_xB_{12}$, are also studied in order to search for a new superconductor in the wide range of new materials.

III. METHOD OF COMPUTATION

To make a theoretical prediction of a novel material, one must determine its stable structure. To make sure whether these compounds really exist or not, the first-principles total energy calculations are performed by means of the *ab initio* pseudopotential[20] Gaussian basis calculation within the local-density-functional theory.[21,22] The details of the calculation are found in our previous paper.[10] The exchange-correlation potential is included via the Perdew-Zunger parametrization[23] of the Ceperley-Alder functional.[24] High numerical precision is achieved by employing a large number of k points (up to 10 points) in 1/12 of the Brillouin zone.

In this calculation, the Bloch functions are expressed by the linear combination of atomic orbitals (LCAO) form. In this LCAO calculation we express the numerically calculated pseudoatomic wave functions in terms of the sum of Gaussian orbitals. In doing so we determine both the coefficients of a linear combination and the exponents of the Gaussian orbitals by the least-squares fit method. When we adopt 19 Gaussian orbitals (3 Gaussians for s-type orbitals, 2 for p types, and 2 for d types, excluding the spin degeneracies) for a single B, Li, or Ca atom, we have found that errors in the least-squares fitting are only within 1% in every kind of atom.

In order to examine the validity of the 19 Gaussian basis sets, we have also tried to fit with 14, 18, and 22 Gaussian orbitals. When the number of Gaussian orbitals per atom exceeds 19, we can reduce the errors in the least-squares fitting below 1%. However, there is ambiguity in choosing a set of Gaussian orbitals. This gives rise to an overcomplete problem. In this context we have concluded that the case of 19 Gaussian orbitals corresponds to the best fitting. Gaussian exponents thus determined are as follows: (a) for a B atom, 0.161, 0.455, and 1.77 as s-type Gaussians, 0.265 and 1.46 as p types, and 0.140 and 0.240 as d types; (b) for a Li atom, 0.043, 0.145, and 0.374 as s types, 0.072 and 0.828 as p types, and 0.073 and 0.177 as d types; and (c) for a Ca atom, 0.043, 0.363, and 5.21 as s types, 0.042 and 0.274 as p types, and 0.242 and 1.98 as d types.

By using these 19N Gaussian basis sets (N is the number of the atoms in a unit cell), we have calculated the energy band structures of bcc Li and fcc Ca metals and we find that our results reproduce well those reported for bcc Li and fcc Ca. This may guarantee the validity that we have adopted the 19N Gaussian orbitals for Li and Ca atoms. In addition, we have also calculated the energy band structure and the lattice constant of α-rh B and compared them with the well-converged plane-wave (PW) basis calculation of Lee, Bylander, and Kleinman,[25] which is considered as the most accurate one in the LDA calculation for α-rh B. The lattice constant and the energy gap in our calculation are 100.1% and 80.5% of experimental values, while those in the PW calculation are 99.2% and 75.3%. Our values are very close to those of the PW calculation and thus our calculations, with the use of the 19N Gaussian basis set for B atoms, are considered as fairly good.

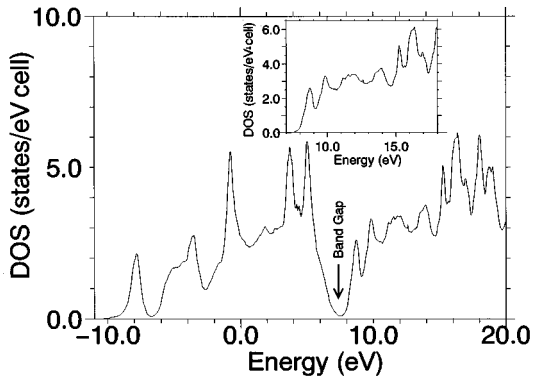

FIG. 2. Calculated density of states of α-rh B. The unoccupied density of states is also given in the inset.

We have further calculated the density of states of α-rh B. The result is shown in Fig. 2. Very recently Terauchi has measured the electron-energy-loss spectra of α-rh B in the energy region of 0–60 eV and with the use of the Kramers-Kronig analysis of the loss function has obtained the real and imaginary parts of the dielectric function.[26] Since the imaginary part of the dielectric function is related to the joint density of states between the occupied deep core states and the unoccupied conduction band states and the deep core state is less dispersive, the density of states of the unoccupied conduction-band states is semiempirically obtained from the electron-energy-loss spectra. In this context we can compare the calculated density of states of α-rh B with the semiempirical one. The agreement with regard to the peak positions between calculated and semiempirical density of states is fairly good, guaranteeing the validity of the 19N Gaussian orbitals for B atoms.

When metal atoms are doped into α-rh B, the structure of α-rh B is deformed. In our previous paper,[10] we have examined this deformation effect in the cases of $Li_2B_{12}(T_d)$ and $Li_2B_{12}(int)$ by calculating the total energies with the $B_{12}P_2$ structure and the α-rh B structure. Of course we have to find an optimized structure for all the model systems, but this calculation is time-consuming. Thus, in the present paper we introduce a pair of structural parameters, the length of the lattice vector a and the mean radius of the icosahedral B_{12} cluster r. We try to minimize the energy by varying these parameters. Since this optimization procedure is too conventional, we must check the validity of this procedure by calculating the atomic force acting on each ion in a re-

TABLE II. Calculated lattice constant a, mean radius of B_{12} r, and bond lengths in α-rh B (Å). The results are compared with experiments and other current calculations.

			B-B bond length					
			intraicosahedron				intericosahedra	
Reference	a	r	t-t (t^*-t^*)	t-e (t^*-e^*)	t-e^* (t^*-e)	$*$ e-e^*	t-t^*	e-e (e^*-e^*)
this work	5.063	1.70	1.74	1.79	1.80	1.78	1.67	2.02
other calc.[a]	5.034		1.741	1.794	1.784	1.773	1.670	2.003
other calc.[b]	5.034		1.740	1.783	1.794	1.772	1.669	2.003
expt.	5.057[c]		1.751[d]	1.782[d]	1.801[d]	1.806[d]	1.670[d]	2.019[d]

[a]Reference 25.
[b]Reference 27.
[c]Reference 18.
[d]Reference 14.

spective compound with the α-rh B structure and with optimized structure. We have found that the forces sharply fall below 10^{-1} a.u. after optimizing the structures. For example, in the optimized $LiB_{12}(O)$, the forces acting on B ions are $0.37\times10^{-2}-0.88\times10^{-1}$ a.u. and that on Li is 0.25×10^{-2} a.u. Thus our procedure of structure optimization by two parameters may be used in various molecularly based crystals, if one would allow the range of remaining forces in an optimized structure to be 10^{-1}–10^{-2} a.u. It should be emphasized that the optimized structures by two parameters are not the most stable structure.

IV. RESULTS

A. Stability and energetics

First of all, calculated structural parameters of α-rh B are summarized in Table II, together with the experimental[13,18] and other available theoretical[25,27] information. Due to the remaining atomic forces on the order of $10^{-3}-10^{-1}$ a.u., insufficient precision (±0.01 Å for α-rh B and ±0.1 Å for Li_xB_{12}) has been achieved in the present calculation.

Also the total energy of isolated atom A (A=Li or Ca) has been calculated for comparison, within the same framework of LDA, employing the same *ab initio* pseudopotentials that we have used in the bulk calculations. The calculations proceeded using numerical bases. In Table III the calculated energy gains ΔE are given for a wide range of metal-doped B_{12} solids. The ΔE is defined by the exothermic reactions $B_{12}(\alpha\text{-rh crystal})+xA(\text{atom})\leftrightarrow A_xB_{12}+\Delta E$. Although the atomic forces still exist in A_xB_{12} even after the minimization, the remaining forces are fortunately the same order in all the A_xB_{12}-type compounds and hence are not considered to have such large effects on the heats of formation ΔE. According to the analysis, Li-doped compounds have been demonstrated to give sufficient heats of formation ΔE, whereas all the Ca-doped compounds have negative ΔE and have been found to be unstable including Li_2CaB_{12}, against our simple rigid-sphere model estimate.

We have also clarified that Li atoms have a preference for the O site rather than the T_d site in Li_xB_{12}, while in the doped C_{60}, alkali atoms prefer T_d sites to O sites.[28] This result is consistent with our estimate by means of a simple rigid-sphere method. Lithium atoms, however, do not occupy the interstitial site and B_{12} center against our model calculation. The *ab initio* total-energy studies also demonstrate that $Li_2B_{12}(int)$ is unstable, though we have calculated both from the α-rh B and $B_{12}P_2$ structures. An intermediate structure, less deviated from the α-rh B structure than $B_{12}P_2$ in proportional to the ratio of Li to P in the ionic radius, has also been adopted as the initial data, but it remains unstable. We have thus concluded that alkali-metal atoms do not occupy interstitial sites, as in the doped C_{60}. Our LDA band-structure calculation reveals the main reason why the $Li_2B_{12}(int)$ has been unstable. According to the

TABLE III. Calculated heats of formation ΔE of A_xB_{12}. $Li_2B_{12}(int)$, $Li@B_{12}$, and all of the Ca-doped A_xB_{12} are unstable, as a minus sign of ΔE shows. $Li_2B_{12}(T_d)$ is metastable. The others are stable enough and should be synthesized like K_xC_{60}.

		ΔE				ΔE	
System	Site	eV/cell	eV/atom	System	Site	eV/cell	eV/atom
$LiB_{12}(O)$	O	2.38	0.183	CaB_{12}	O	-7.23	-0.556
$Li_2B_{12}(T_d)$	T_d	2.29	0.164	Ca_3B_{12}	$O+T_d$	-51.13	-3.409
$Li_2B_{12}(int)$	int	-2.70	-0.193	Li_2CaB_{12}	O(Ca)$+T_d$(Li)	-3.20	-0.213
$Li@B_{12}$	B_{12} center	-2.86	-0.220				
				KC_{60}	T_d	8.5	0.139
Li_3B_{12}	$O+T_d$	4.63	0.309	K_2C_{60}	T_d	17.7 [a]	0.285
$Li@Li_3B_{12}$	$O+T_d+B_{12}$ center	2.92	0.182	K_3C_{60}	$O+T_d$	22.6 [a]	0.359

[a]Reference 28.

calculations, all stable and metastable Li_xB_{12} are ''donor-type'' metals, as seen in Sec. IV A, but the calculated energy band structure of unstable $Li_2B_{12}(int)$ instead shows an ''acceptor-type'' metallic behavior.[9,10] Since some p_π orbitals point towards interstitial sites, the Li $2s$ wave function in $Li_2B_{12}(int)$ overlaps substantially with these p_π orbitals and as a result, two Li-B hybrid bands appear in the higher valence band region of α-rh B. Because they push up higher valence bands, E_F crosses the highest and second-highest valence bands and holelike carriers appear in this case, indicating which Li gets an extra electron and behaves as an anion in $Li_2B_{12}(int)$. This unusual behavior yields anomalously high total energy, that leads to the instability of $Li_2B_{12}(int)$.

From a comparison between the calculated heats of formation ΔE, we can consider the $LiB_{12}(O)$ as a stable stoichiometric phase as long as the Li concentration remains in a lower level. When the Li concentration is increased, the stoichiometric Li_3B_{12} appears. The Li_3B_{12} is the most stable compound among Li_xB_{12}, because of the largest ΔE of approximately 0.309 eV/atom. As seen in Table III, it is a comparable value to that of the already obtained stable material K_3C_{60} (Ref. 28) and this comparison authorizes the existence of Li_3B_{12}. When Li concentration is further increased, $Li@Li_3B_{12}$ is obtained. It corresponds to the maximum concentration, for interstitial sites are too close to O sites and the occupation of interstitial sites by additional Li atoms do not occur because other Li atoms have already occupied the O sites.

B. Band structure

The calculated energy band structures of the stable and metastable Li_xB_{12} ($x=1-4$) are presented in Fig. 3. The LDA band calculation indicates that the general features of energy bands in Li_xB_{12} are mostly attributed to the band profile of α-rh B. The energy band structure of α-rh B is shown in Fig. 3(a). The undoped α-rh B is an indirect semiconductor with the gap energy of approximately 2 eV.[17] The calculated energy band structure of α-rh B within LDA compares quite well with experiments,[17] though the calculated band gap shows a smaller energy value of 1.53 eV. We have also compared it with other LDA calculations[29,30] and have found reasonable agreement with them. The top of the valence band is located at Z and the bottom of the conduction band is at the Γ point. However, the highest occupied valence band is less dispersive along the Γ-Z direction and one may regard α-rh B as an almost direct gap semiconductor. Although this highest valence band exhibits flat dispersion along the Γ-Z direction, it shows a dispersive feature along the Γ-L direction, suggesting a strong anisotropy near the Γ point. No localized electronic states appear as the ground states of α-rh B, though many experiments suggest the existence of intrinsic acceptor levels in β-rh B.[31]

Figure 3(b) shows the calculated energy band structure of $LiB_{12}(O)$. Overall energy band features of $LiB_{12}(O)$ are almost identical to those of α-rh B, but a Li-character band appears in a higher-energy region above 20 eV beyond the displayed range in Fig. 3(b). Lithium $2s$ electrons are transferred from this band to the lowest conduction band and, as a consequence, the Fermi level E_F crosses this lowest conduc-

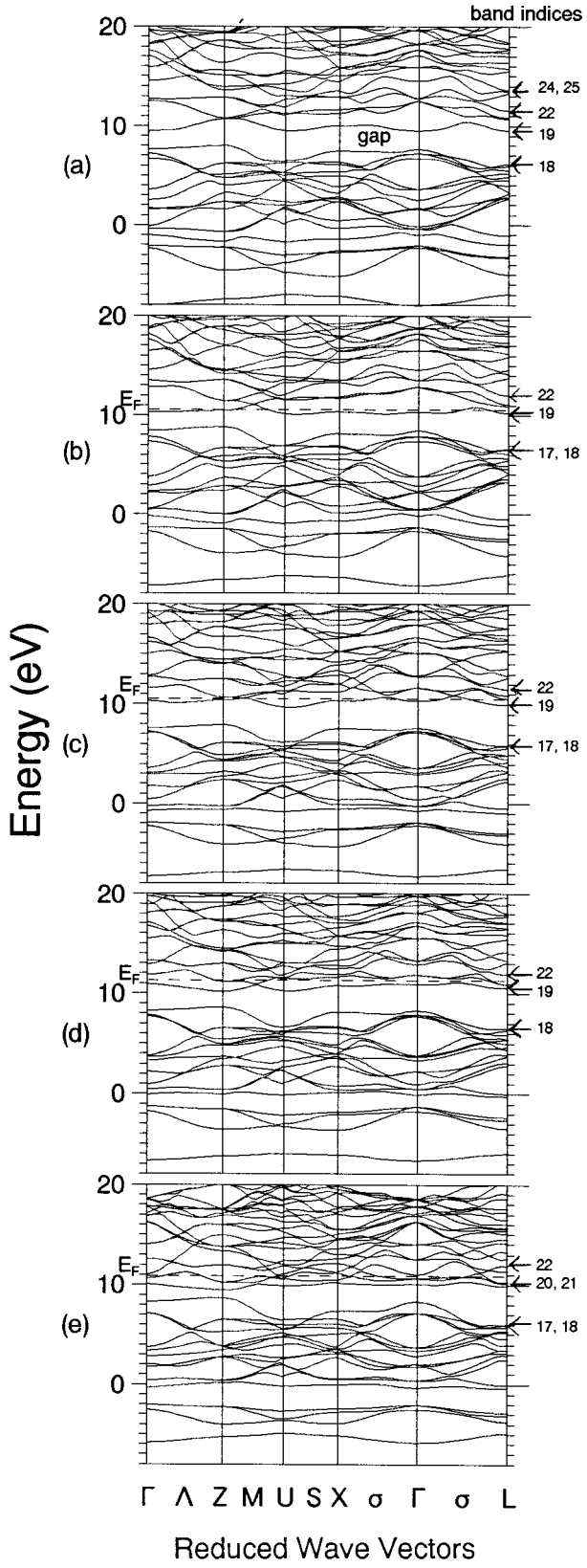

FIG. 3. Calculated energy band structure of semiconducting α-rh B and metallic compounds Li_xB_{12} ($x=1-4$): (a) α-rh B, (b) the stable $LiB_{12}(O)$, (c) the metastable $Li_2B_{12}(T_d)$, (d) the most stable Li_3B_{12}, and (e) the stable $Li@Li_3B_{12}$. The band indices are numbered from the lowest band.

tion band and $LiB_{12}(O)$ shows a donor-type metallic behavior. This band is nearly half filled and all of the donated charges (one electron per B_{12}) are itinerant. Our charge density calculations also reveal that this band has B $2s$-$2p$ hybridized character. This B $2s$-$2p$ conduction band extends in the narrow region between 10.2 and 11 eV, while in the pristine α-rh B, the corresponding band lies in the range between 9.5 and 11 eV. The same kind of narrowing of bandwidths occurs in several bands. It arises from the smaller orbital overlaps, due to both the intra- and intermolecular relaxations. In addition to the narrow bandwidth of the lowest conduction band (of order approximately 0.8 eV), most of its energy dispersion is almost flat in the neighborhood of E_F and a very strong peak appears in the density of states at E_F, as seen in Sec. IV C. This will be very advantageous to the occurrence of superconductivity.

The calculated energy band structure of the metastable $Li_2B_{12}(T_d)$ is shown in Fig. 3(c). Charge transfer similar to the previous case is brought about by doping. From the analysis of the charge-density distribution at the Γ point, we notice that the 22nd conduction band has some Li $2s$ character, whose position is approximately 2 eV above E_F. This band originally had B $2s$ character. The corresponding band in α-rh B is the 24th in Fig. 3(a), but has moved down through the hybridization with Li $2s$ character in Li_2B_{12} (T_d). A charge-density peak of this band appears just on the Li atom, but these electrons are transferred into two lower bands: the 19th B $2s$-$2p$ hybridized band and the 20th B $2p$ band with a little admixture of Li $2s$ character. As the result of charge transfer, E_F crosses the lowest 19th and the second lowest 20th conduction bands and $Li_2B_{12}(T_d)$ also shows metallic behavior. The lowest $B2s-2p$ hybridized conduction band is almost filled, but it yields a few holelike carriers around σ point. The second lowest B $2p$ conduction band is occupied a little, but a low concentration of electrons is found around the Z and L points. The calculated energy band structure has demonstrated that the metastable Li_2B_{12} (T_d) metallic system has two types of charged carriers in the same order. A band gap of about 1.7 eV exists in Li_2B_{12} (T_d) below the two partially occupied conduction bands. The gap has changed its character from direct in α-rh B to indirect, where the ''top'' of valence bands in $Li_2B_{12}(T_d)$ is at the Z point and the ''bottom'' of conduction bands locates at the U point. In the case of $LiB_{12}(O)$, the almost direct gap of approximately 1.5 eV is open and not changed so much as compared to α-rh B.

The calculated energy band structures of the most stable Li_3B_{12} is shown in Fig. 3(d), where Li atoms are doped both into O and T_d sites. Results similar to previous cases have been obtained. Associated with considerable hybridization with a Li $2s$ character band, the 22nd band has moved farther down into the energy region between 11.7 and 13.5 eV, whose position is about 1 eV above E_F. From the 22nd B $2s$-Li $2s$ strongly hybridized band, Li $2s$ electrons are transferred into the lower 19th, 20th, and 21st bands. Due to higher Li concentration, much more electrons than in previous cases are transferred and the 19th band is completely filled. The E_F crosses the almost degenerate 20th and 21st conduction bands in Li_3B_{12}. Sufficient electrons are doped into these bands and they occupy **k** states around the Z and L points. These bands originally had B $2p$ character in undoped α-rh B, but in Li_3B_{12}, B $2p$ character is mixed with Li $2s$ character in almost a one-to-one ratio. In this way, the donor type metallic state is obtained as the ground state of Li_3B_{12} and one can say that there are some similarities in the electronic structure as well as in the crystalline structure between the most stable Li_3B_{12} and the superconducting A_3C_{60}.

A striking feature appears in the case of $Li@Li_3B_{12}$, where its energy band structure is shown in Fig. 3(e). The originally B $2s$ character band, whose energy range in α-rh B lies between 13 and 15 eV (the 24th band in α-rh B), is now considerably hybridized with Li $2s$ character and appears in the region from 10.5 to 12 eV in $Li@Li_3B_{12}$. In this region, there already exist two almost degenerate B $2p$-Li $2s$ character bands, and these three bands interact with one another. As a result, the 20th band has dominant Li $2s$ character along the U-X direction with a little admixture of B $2s$ character, whereas it has B $2p$-Li $2s$ character for other **k** points in the Brillouin zone. As for the 22nd band, quite the contrary occurs. Besides these changes, the 19th valence band that is fully occupied by the transferred Li $2s$ electrons is lowered and the Fermi energy decreases in spite of the increase of Li concentration. The E_F crosses the 20th and 21st conduction bands. Since the 20th band has Li $2s$ character along the U-X direction, the electrons in this region remain around Li ions and do not transfer to other B character bands.

C. DOS

The knowledge of the density of states (DOS) $N(E)$ near the Fermi level is very important in understanding a mechanism of superconductivity. In order to investigate the possibility of superconductivity in Li_xB_{12} metallic materials, $N(E)$ has been calculated and is delineated in Fig. 4 for pristine and doped α-rh B. The Fermi-level DOS $N(E_F)$ is also given in Table IV, together with a calculated value of superconducting K_3C_{60} within the LDA.[28,32] The tetrahedron method[33] is used in actual calculation of $N(E_F)=\Sigma_n\Sigma_{\vec{k}}\delta(E_F-\varepsilon_n(\vec{k}))$.

Since in $LiB_{12}(O)$ the lowest B $2s$-$2p$ conduction band that crosses E_F is almost flat, this single narrow band yields a pronounced spike structure in $N(E)$ at E_F, which is expected to play an important role in superconductivity. Although a number of LDA calculations on $N(E_F)$ of the K_3C_{60} have been reported so far, the calculated $N(E_F)$ is not definite yet, ranging from 0.19 to 0.39 states/eV atom.[28,32] The value of $N(E_F)$ per atom in $LiB_{12}(O)$ is comparable to the moderate $N(E_F)$ of K_3C_{60}, as seen in Table IV.

In $Li_2B_{12}(T_d)$, its energy band structure is similar to that of $LiB_{12}(O)$ and only minute differences in $N(E)$ are found. However, because of the large amount of charge transfer, E_F lies at a little higher level away from the B $2s$-$2p$ hybridized conduction band and $N(E_F)$ decreases compared to $LiB_{12}(O)$.

In Li_3B_{12}, the amount of charge transfer increases much more than in the two previous cases and E_F, whose energy position is 11.4 eV, crosses two higher almost-degenerate B $2p$-Li $2s$ hybridized conduction bands and as a consequence $N(E_F)$ becomes again very high. The most stable Li_3B_{12}

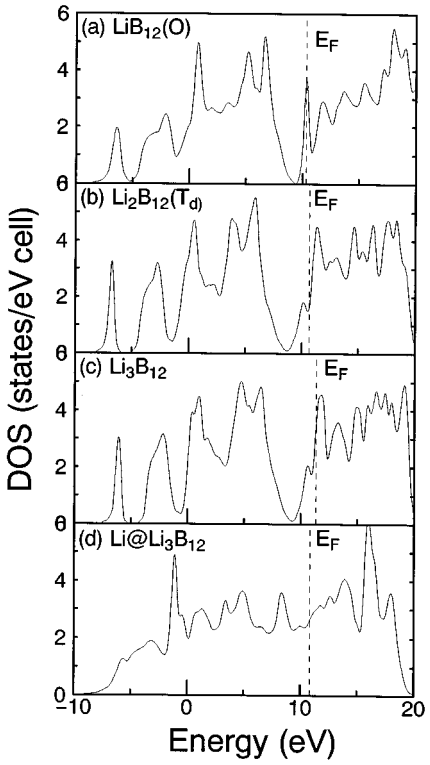

FIG. 4. Calculated density of states of the stable and metastable metallic compounds Li_xB_{12} ($x=1-4$).

matches, or even surpasses, the superconducting K_3C_{60} in the obtained value of $N(E_F)$ per atom.

In $Li@Li_3B_{12}$, E_F instead takes a lower value of about 10.8 eV, contrary to the increase of Li concentration. The decrease of the Fermi energy is related to the lowering of bands, as mentioned in Sec. IV B. The DOS structure of $Li@Li_3B_{12}$ is also changed drastically. The E_F crosses the almost degenerate 20th and 21st bands, but the obtained $N(E_F)$ is not so high compared to $LiB_{12}(O)$ or Li_3B_{12}.

Lithium doping yields changes in $N(E_F)$ according to the band occupation of transferred electrons, as mentioned above. With the exception of the metastable $Li_2B_{12}(T_d)$, Li_xB_{12} ($x=1-4$) mostly shows a high density of states at E_F. Higher values of $N(E_F)$ are mainly due to the nature of the lowest and second-lowest conduction bands of the parent

TABLE IV. Obtained DOS at E_F of stable and metastable Li_xB_{12}. A LDA calculation of $N(E_F)$ for superconducting K_3C_{60} is referred to for comparison.

System	$N(E_F)$ states/eV cell	$N(E_F)$ states/eV atom
$LiB_{12}(O)$	3.39	0.26
$Li_2B_{12}(T_d)$	1.59	0.11
Li_3B_{12}	3.78	0.25
$Li@Li_3B_{12}$	2.55	0.16
K_3C_{60}	17.96[a]	0.28

[a]Reference 32. The calculated values of $N(E_F)$ are ambiguous, ranging from 12.0 to 25.0 states/eV cell (Refs. 28 and 32). Here we have referred to a moderate value.

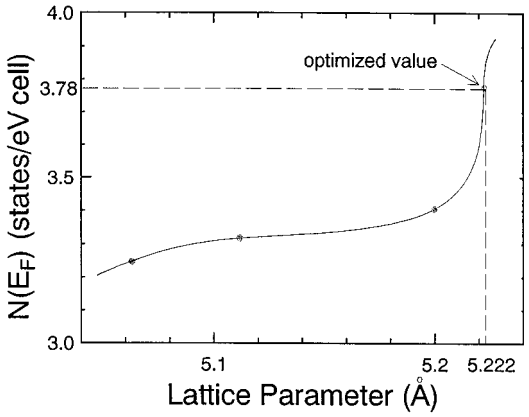

FIG. 5. Calculated $N(E_F)$ of Li_3B_{12} as a function of the lattice constant a. No simple linear relation exists in Li_xB_{12}, but the obtained $N(E_F)$ (solid circles) shows a monotonic increase at least in this region.

α-rh B. The $N(E_F)$ is also enhanced by the narrowing of the energy bandwidths associated with Li doping.

In A_xC_{60}, there exists an approximate linear relationship between $N(E_F)$ and the lattice constant and the variation in T_c has been attributed to changes in the lattice constant. In Li_xB_{12}, however, no such simple linear relation exists, reflecting the intermolecular-covalent-bonding-type cohesion, but the calculated $N(E_F)$ shows a monotonic increase as a function of the lattice constant. Figure 5 illustrates the calculated $N(E_F)$ of Li_3B_{12} as a function of the lattice constant a. The $N(E_F)$ has been enhanced by 16.7% in the optimized structure, compared to the unrelaxed structure. It also indicates that Li_3B_{12} would show a high value of T_c with the help of low pressure, affected by the rapid increase in $N(E_F)$.

D. Bulk modulus

The bulk modulus of the stable and metastable materials has also been calculated for some information about isotropic phonon mode. The calculated bulk modulus is given in Table V for α-rh B and its stable and metastable derivatives Li_xB_{12} ($x=1-4$). The bulk modulus of α-rh B shows excellent agreement with an x-ray single-crystal study of α-rh B.[34]

As seen in Table V, the bulk modulus initially increases by the doping, but then it decreases monotonically with increasing Li concentration. The initial increase in the bulk modulus is attributed to additional contributions from the ion-ion electrostatic interaction associated with doping. One might consider that the formation of metallic bondings, to which the interactions of conduction electrons with Li^+ ions mainly contribute, may also be responsible for it, but it is less important because the present total-energy calculation shows that the Ewald sum contribution due to electrostatic interactions is dominant rather than the band energy contribution. The reason for the behavior of monotonic decreasing is that dopant Li^+ ions weaken the intermolecular covalent bondings via the relaxations of inter-B_{12} clusters. As a result, the bulk moduli of $Li@Li_3B_{12}$ and Li_3B_{12} are comparable to that of undoped α-rh B, which is indicative of the same order of phonon frequencies.

TABLE V. Optimized lattice constant a and calculated bulk modulus B around the optimized geometry of α-rh B and Li_xB_{12}. Other available LDA calculation of B for fcc C_{60} and K_3C_{60} are referred to for comparison.

System	a (Å)	B (GPa)
α-rh B	5.063	233
$LiB_{12}(O)$	5.077	417
$Li_2B_{12}(T_d)$	5.200	365
Li_3B_{12}	5.222	325
$Li@Li_3B_{12}$	5.404	242
C_{60}	9.64[b]	48[c]
K_3C_{60}	9.44 [b]	29[c]

[a]The present LDA calculation overestimates the lattice constant a only by 1.1% and the obtained values of a and hence of the bulk modulus B compare quite well with experiments (Refs. 13 and 34).
[b]Lattice constant in rhombohedral description, derived from Ref. 28.
[c]Reference 28.

X-ray diffraction studies on α-rh B and B_{12}-based crystals[13,14] have revealed that a B_{12} cluster is distorted from a regular icosahedron by the Jahn-Teller effect.[31,35] In addition, a higher Debye temperature in α-rh B of approximately 1430 K is also derived[36] from specific heat capacity measurements on β-rh B and $B_{12}C_3$.[37] These studies suggest that there exists an anomalously strong electron-phonon interaction between valence electrons and some vibrational modes in α-rh B. Because the phonon frequencies are almost unaffected by doping, even after the doping, strong electron-phonon coupling is also expected, suggesting a future discovery of new superconductors in Li_xB_{12}.

V. SUMMARY AND CONCLUSION

We have theoretically predicted the possible existence of B_{12}-based new materials Li_xB_{12}, with $x=1-4$, on the basis of the first-principles calculations within the LDA. However, our total-energy calculations have also demonstrated that Ca_xB_{12}, with $x=1-4$, is unstable. Among the stable Li_xB_{12}, the Li_3B_{12} compound, with the same stoichiometry as the superconducting A_3C_{60}, is the most stable. Our calculations may suggest that the doping of α-rh B with Li atoms can be achieved experimentally in a usual gas transport technique. The stoichiometry will be controlled by the temperatures, pressures, duration of the reactions, and the number of moles of Li relative to those of α-rh B.

Our band-structure calculations have revealed essentially donor-type metallic behavior of Li_xB_{12}. From an analysis of the energy band profile, we have pointed out that Li-doping produces changes that can be related to the dopant concentration, particularly in the bands near the Fermi level. These changes are advantageous to $LiB_{12}(O)$ and Li_3B_{12} and these two compounds show a high density of states at E_F, comparable to K_3C_{60} in the value of per atom. As regards Li_3B_{12} and $Li@Li_3B_{12}$, we have also clarified that Li doping does not cause any drastic changes in the bulk modulus. The observed Jahn-Teller effect and high Debye temperature in α-rh B are also expected in these compounds, which is indicative of an anomalously strong electron-phonon coupling strength.

For many desired properties as a superconductor, Li_3B_{12} has both the high density of states at E_F and the strong electron-phonon coupling. Thus a moderately high value of T_c is expected, mediated by the interaction of conduction electrons with high-frequency phonons caused by B-B covalent bondings. In this context, the most stable Li_3B_{12} is a promising candidate for a new superconductor based on semiconducting materials.

ACKNOWLEDGMENTS

The authors are very grateful to Dr. Terauchi for showing their EELS data of α-rh B prior to publication. This work was partly performed under the Project for Parallel Processing and Super Computing at Computer Centre University of Tokyo. Financial support was provided by a Grant-in-Aid from Ministry of Education, Science and Culture of Japan. One of the authors (S. G.) also acknowledges the Japan Society for the Promotion of Science.

*Present address: Institute of Physics, University of Tsukuba, Ibaraki 305, Japan.

[1] R. J. Cava *et al.*, Nature (London) **367**, 6459 (1994).
[2] Y. Iwasa *et al.*, Science **264**, 5165 (1994).
[3] G. Oszlanyi and L. Forro, Solid State Commun. **93**, 4 (1995).
[4] R. Naslain, A. Guette, and P. Hagenmuller, Less Common Met. **47**, 1 (1976).
[5] J. L. Hoard, in *Boron*, edited by J. A. Kohn *et al.* (Plenum, New York, 1960), Vol. 1, p. 1.
[6] D. B. Sullenger and Ch. L. Kennard, Sci. Am. **215**, 7 (1966).
[7] C. E. Holcombe, Jr. *et al.*, High Temp. Sci. **5**, 349 (1973).
[8] P. Runow, J. Mater. Sci. **7**, 499 (1972).
[9] S. Gunji, H. Kamimura, and T. Nakayama, in *Proceedings of the 21st International Conference on Physics of Semiconductors, Beijing, 1993*, edited by Xie Xide, Kun Huang, and L.L. Chang (World Scientific, Singapore, 1993), p. 1832.
[10] S. Gunji, H. Kamimura, and T. Nakayama, J. Phys. Soc. Jpn. **62**, 2408 (1993).
[11] S. Gunji and H. Kamimura, Jpn. J. Appl. Phys. Ser. **10**, 35 (1994).
[12] S. Gunji and H. Kamimura, in *Proceedings of the 22nd International Conference on Physics of Semiconductors, Vancouver, 1995*, edited by D. J. Lockwood (World Scientific, Singapore, 1995), p. 2185.
[13] D. R. Tallant, T. L. Aselage, A. N. Campbell, and D. Emin, Phys. Rev. B **40**, 5649 (1989).
[14] B. Morosin, A. W. Mullendore, D. Emin, and G. A. Slack, in *Boron-Rich Solids*, edited by D. Emin, T. L. Aselage, C. L. Beckel, I. A. Howard, and C. Wood, AIP Conf. Proc. No. 140 (AIP, New York, 1986), p. 70.
[15] G. A. Slack, T. F. McNelly, and E. A. Taft, J. Phys. Chem. Solids **44**, 1009 (1983); T. L. Chu and A. E. Hyslop, J. Electrochem. Soc. **121**, 412 (1974).
[16] H. Werheit, H. Binnenbruck, and A. Hausen, Phys. Status Solidi B **47**, 153 (1971).
[17] F. H. Horn, J. Appl. Phys. **30**, 1611 (1959); E. P. Domashevskaya *et al.*, Less Common Met. **47**, 189 (1976).

[18] B. F. Decher and J. S. Kasper, Acta Crystallogr. **12**, 503 (1959).
[19] L. Pauling, *The Nature of the Chemical Bond*, 3rd ed. (Cornell University Press, Ithaca, 1966).
[20] D. R. Hamann, M. Schlüter, and C. Chiang, Phys. Rev. Lett. **43**, 1494 (1979); G. B. Bachelet, D. R. Hamann, and M. Schlüter, Phys. Rev. B **26**, 4199 (1982).
[21] P. Hohenberg and W. Kohn, Phys. Rev. **136**, B864 (1964).
[22] W. Kohn and L. J. Sham, Phys. Rev. **140**, A1133 (1965).
[23] J. Perdew and A. Zunger, Phys. Rev. B **23**, 5048 (1981).
[24] D. M. Ceperley and B. J. Alder, Phys. Rev. Lett. **45**, 566 (1980).
[25] S. Lee, D. M. Bylander, and L. Kleinman, Phys. Rev. B **42**, 1316 (1990).
[26] M. Terauchi (private communication).
[27] D. Li, Y. N. Xu, and W. Y. Ching, Phys. Rev. B **45**, 5895 (1992).
[28] S. Saito and A. Oshiyama, Phys. Rev. B **44**, 11 536 (1991); A. Oshiyama, S. Saito, N. Hamada, and Y. Miyamoto, J. Phys. Chem. Solids **53**, 1457 (1992).
[29] T. Hatakeyama and H. Kamimura, in *Surface Physics and Related Topics. Festschrift for Xie Xide*, edited by Fu-jia Yang *et al.* (World Scientific, Singapore, 1991), p. 166; in *Proceedings of the 20th International Conference on Physics of Semiconductors*, edited by E. M. Anastassakis and J. D. Joannopoules (World Scientific, Singapore, 1991), p. 730; T. Hatakeyama, in *New Horizons in Low-Dimensional Electron Systems. Festschrift for Hiroshi Kamimura*, edited by H. Aoki *et al.* (Kluwer, Dordrecht, 1992), p. 433.
[30] L. Kleinman, in *Boron-Rich Solids*, edited by D. Emin, T. L. Aselage, A. C. Switendick, B. Morosin, and C. L. Beckel (AIP, New York, 1991), p. 13; S. Lee, D. M. Bylander, and L. Kleinman, Phys. Rev. B **42**, 1316 (1990).
[31] H. Werheit, M. Laux, and U. Kuhlmann, Phys. Status Solidi B **176**, 415 (1993); R. Franz and H. Werheit, Europhys. Lett. **9**, 145 (1989).
[32] M. Z. Huang, Y. N. Xu, and W. Y. Ching, Phys. Rev. B **46**, 6572 (1992), and related references therein.
[33] J. Rath and A. J. Freeman, Phys. Rev. B **11**, 2109 (1975).
[34] R. J. Nelmes, J. S. Loveday, D. R. Allan, J. M. Besson, G. Hamel, P. Grima, and S. Hull, Phys. Rev. B **47**, 7668 (1993).
[35] R. Franz and H. Werheit, in *Boron-Rich Solids*, AIP Conf. Proc. No. 231 (Ref. 30), p. 29 and related references therein.
[36] G. A. Slack, D. W. Oliver, and F. H. Horn, Phys. Rev. B **4**, 1714 (1971).
[37] G. A. Slack, Phys. Rev. **139**, A507 (1965).